Structural Investigation of Star Polymers in Solution by Small Angle Neutron Scattering

L. Willner,*,† O. Jucknischke,† D. Richter,† J. Roovers,‡ L.-L. Zhou,‡ P. M. Toporowski,‡ L. J. Fetters,§ J. S. Huang,§ M. Y. Lin,§ and N. Hadjichristidis∥

Institut für Festkörperforschung, Forschungszentrum Jülich GmbH, 52425 Jülich, Germany, Institute for Environmental Chemistry, National Research Council, Ottawa, Ontario, Canada K1A OR6, Exxon Research & Engineering Company, Annandale, New Jersey 08801, and Department of Chemistry, The University of Athens, 15771 Athens, Greece

Received January 17, 1994; Revised Manuscript Received April 19, 1994®

ABSTRACT: Using small angle neutron scattering, we investigated the conformation of star polymers with functionalities ranging from $f = 8$ to $f = 128$ in a good solvent. The stars were made by anionic polymerization of isoprene or butadiene using multifunctional chlorosilane linking agents. Single star form factors at zero concentration were determined by extrapolating low concentration data to $\phi = 0$. Conformations at finite concentrations were obtained by the zero average contrast method. In general the star form factors are well described in terms of the Daoud–Cotton scaling model. This concerns the molecular weight, functionality, and concentration dependence of R_G as well as the shape of the form factor. In particular the step height between the low Q and asymptotic power law regime was found to follow an $f^{3/2}$ law. Furthermore, with increasing functionality the star form factors were found to tend toward spherelike behavior, bearing evidence for a secondary maximum at the position of the third oscillation of the corresponding sphere form factor.

1. Introduction

The static scattering behavior of regular star polymers in solution has been the subject of numerous experimental investigations during recent years. Light scattering, small angle neutron scattering (SANS), and X-ray scattering techniques were applied to examine structural aspects[1–11] as well as some special features of star polymer interactions, leading to ordering phenomena around the overlap concentration.[2,9,12,13]

However, experiments performed thus far are restricted to molecules with relatively low functionalities, since regular stars possessing more than 18 arms had not been synthesized. Recently, Roovers et al.[14,15] succeeded in the synthesis of 32, 64, and 128 arm stars via the preparation of well-defined high functionality chlorosilane linking agents. In the present paper we report SANS measurements on star polymers with functionalities of $f = 8$, 18, 32, 64, and 128 in a good solvent.

We have concentrated on a systematic investigation of the single star form factor, $P(Q)$, as a function of f and molecular weight. Determination of $P(Q)$ was made in the limit of infinite dilution. Additionally, we have examined the concentration dependence of $P(Q)$ for two stars with 18 and 64 arms. For this purpose we have used the zero average contrast method.[16] This method is a special labeling technique which allows the direct measurement of form factors at finite concentrations since contributions from interparticle interactions cancel. Thereby a higher scattering intensity is obtained compared to the method where only a small amount of labeled polymer is measured in a matrix of unlabeled polymer and solvent.

From the theoretical point of view star polymers have gained considerable interest because they serve as prototype examples for tethered chains, polymer brushes, and multibranched systems. Following Gaussian chain statistics, Benoit[17] derived a single star form factor in 1953. In order to incorporate the influence of the excluded volume interaction Allessandrini and Carignano[18] recently calculated the static scattering function with renormalization group techniques. They provide a best nonlinear fit of the theoretically derived function which allows a comparison with experimental data up to 18 arms. A conformational study of star polymers in a good solvent via a self-consistent minimization of the intramolecular free energy was reported by Allegra et al.[19] Moreover, the conformation of stars was examined by Daoud and Cotton[20] and Birshtein et al.[21,22] using scaling concepts. The proposed model is based on a blob picture common to semidilute solutions. Due to the inhomogeneous density distributions in stars, the size of the blobs increases on passing from the center to the rim. Grest et al.[23] have presented a detailed molecular dynamics (MD) simulation study of star polymers with relatively few monomers but many arms. In most respects they obtained good agreement with the scaling predictions of the blob model.

In this work we present our data in light of the different theoretical approaches. Scaling predictions, in particular the size dependence on functionality and molecular weight, will be checked by our experimental results. By comparison to a hard sphere form factor we demonstrate the increasingly spherelike constant density distributions at higher degrees of branching.

We further concentrate on an analytical description for the star form factors. Thereby it will be shown that we can approximate our data by an equation consisting of two contributions: One represents a shape function arising from the density correlations of the whole star and the second term is given by the Fourier transform of the pair correlation function of a polymer in a blob. Finally, we will discuss the concentration dependence of the form factors in the dilute and semidilute range. For the 18 arm star we found scaling properties which are analogous to those of linear polymers. In contrast the 64 arm star behaves entirely differently. Here it will be shown that

* To whom correspondence should be sent.
† Institut für Festkörperforschung.
‡ Institute for Environmental Chemistry.
§ Exxon Research & Engineering Co.
∥ The University of Athens.
® Abstract published in *Advance ACS Abstracts,* June 1, 1994.

0024-9297/94/2227-3821$04.50/0

Table 1. Molecular Weights of Star Polymers and Single Arms

		$10^{-3}M_{W,star}$		$10^{-3}M_{N,arm}$	
sample[a]	f	SANS[b]	LS[c]	osmometry	SEC[d]
PB12807	128	715	840	6.8	
PB6415	64	774	725	12.1	
PB6407	64	405	395	6.3	
PB3237	32		1330	37.4	
PB3220	32		644	19.4	
PB3210	32	256	301		9.5
PB3205	32	168	169[e]		5.4
PI18	18	134	138		7.5
PI8	8	66	61		7.5
PB6407D	64				7.0
PI18D	18				8.4

[a] PB = polybutadiene, PI = polyisoprene, D = deuterated. [b] By Zimm analysis. [c] By light scattering in cyclohexane. [d] By calibration with linear PB and PI, respectively. [e] 1.55×10^5 by osmometry.[14]

the change in $P(Q)$ with concentration is not due to a shrinkage of the molecule but must have other origins.

2. Experimental Section

The 8 and 18 arm stars were made of polyisoprene (PI), while the stars with 32, 64, and 128 arms were built from polybutadiene (PB). The detailed synthesis of the star polymers was described elsewhere.[14,15,24,25] First a narrow molecular weight linear living polydiene was prepared by anionic polymerization techniques with *s*-BuLi as the initiator. A small fraction was removed and terminated with degassed methanol. It is the reference arm material. The polymerization conditions used led to a statistically uniform stereoirregular chain microstructure (for PI, ~7 wt % 3,4, ~70 wt % *cis*-1,4, ~23 wt % *trans*-1,4; for PB, ~8 wt % 1,2, ~50 wt % *cis*-1,4, ~42 wt % *trans*-1,4). The living polydiene was reacted with the appropriate multifunctional chlorosilane compound. The 8 arm star was prepared by linking of the arms with $Si[CH_2CH_2Si(CH_3)Cl_2]_4$, and the 18 arm star was obtained with $[CH_2Si(CH_2CH_2SiCl_3)_3]_2$.

Dendrimer carbosilanes containing 32, 64, and 128 silicon–chlorine bonds in the perimeter have been prepared and have been used as linking agents to prepare 32, 64, and 128 arm star polybutadienes. The chlorosilane dendrimers were synthesized from the corresponding vinyl compound by hydrosilylation with methyldichlorosilane in the presence of a platinum catalyst. The starting compound was the tetravinylsilane. The synthesis and properties of the vinylcarbosilane and chlorocarbosilane dendrimers has been described previously.[24-26] A 2–3-fold excess of living polydiene was used in order to force the linking reaction to completion. The linking reaction was monitored by comparison of the high molecular weight star peak and the low molecular weight arm peak of the size exclusion chromatograph (SEC) traces. The excess of the living linear polymer was terminated with degassed methanol. The star polymers were extensively fractionated in a benzene (or toluene)–methanol mixture in order to remove the excess of the arm material. All polymer solutions were protected against oxidation, degradation, and cross-linking by 4-methyl-2,6-di-*tert*-butylphenol. For the zero average contrast experiment two deuterated stars, PB6407D and PI18D, were prepared in order to match the corresponding protonated stars in functionality and molecular volume.

The number average molecular weight M_N of the precursor polymer was measured with a Hewlett-Packard 503 osmometer in toluene at 35 °C or by SEC, calibrated with linear polyisoprenes and polybutadienes in tetrahydrofuran at 30 °C. Elution volumes of the deuterated and protonated precursor polymers were almost identical. Molecular weights of the deuterated arms were therefore estimated to be higher by a factor of 1.12 (PI) and 1.11 (PB) due to the ratio of molecular weights of deuterated and protonated monomers, respectively. The weight average molecular weight of the star polymers was measured in cyclohexane at 25 °C by light scattering with a Brookhaven system or with a Chromatix KMX-6 low angle laser photometer. The molecular characteristics are summarized in Table 1.

The coherent macroscopic scattering cross section, $d\Sigma(Q)/d\Omega$, of a SANS experiment can be defined in the following way:

$$\frac{d\Sigma}{d\Omega}(Q) = \frac{\Delta\rho^2}{N_A}S(Q) \tag{1}$$

Here Q is the scattering vector given by $4\pi \sin(\theta/2)/\lambda$ where θ is the scattering angle and λ the neutron wavelength. N_A denotes the Avogadro constant, and $S(Q)$, the static scattering function. $\Delta\rho^2$ is the contrast factor given by

$$\Delta\rho^2 = \left(\frac{\Sigma b_P}{v_P} - \frac{\Sigma b_S}{v_S}\right)^2 \tag{2}$$

where Σb_S and Σb_P are the coherent scattering lengths and v_S and v_P the volumes of the solvent molecule and the repeat unit, respectively.

In the case of dilute polymer solutions the inverse scattering function can be expressed by the following equation:

$$\frac{\phi}{S(Q)} = \frac{1}{V_W P(Q)} + 2A_2\phi \tag{3}$$

where $P(Q)$ is the polymer form factor. V_W denotes the weight average molar polymer volume, ϕ the monomer volume fraction, and A_2 the second virial coefficient.

In order to measure the polymer form factor at higher concentrations an experiment under zero average contrast conditions can be used.[16,27-29] Thereby a 50 vol % blend of a deuterated and a protonated polymer, both of the same volume, is investigated in a mixture of deuterated and protonated solvent having the same average scattering length density ρ_0:

$$\rho_0 = \frac{1}{2}\left(\frac{\Sigma b_{P,H} + \Sigma b_{P,D}}{v_P}\right) = \frac{\phi_H \Sigma b_{S,H} + (1-\phi_H)\Sigma b_{S,D}}{v_S} \tag{4}$$

with ϕ_H as the volume fraction of the protonated solvent. According to eq 1 the scattering cross section can be expressed as the sum of partial scattering functions:

$$\frac{d\Sigma}{d\Omega}(Q) = \frac{1}{N_A}(\Delta\rho_H{}^2 S_{HH} + \Delta\rho_D{}^2 S_{DD} + 2\Delta\rho_H\Delta\rho_D S_{DH}) \tag{5}$$

with indices D and H referring to deuterated and protonated monomers, respectively. Under zero average contrast conditions

$$\Delta\rho_z = \Delta\rho_D = -\Delta\rho_H = \frac{\Sigma b_{P,D}}{v_P} - \rho_0 \tag{6}$$

eq 5 can be rewritten as

$$\frac{d\Sigma}{d\Omega}(Q) = \frac{\Delta\rho_z{}^2}{N_A}(S_{HH} + S_{DD} - 2S_{DH}) \tag{7}$$

If we introduce the decomposition of the partial scattering functions into a self-contribution (I) and a distinct contribution (II) according to

$$S_{ij} = S_i{}^I\delta_{ij} + S_{ij}{}^{II} \tag{8}$$

where i and j denote H and D, one obtains

$$\frac{d\Sigma}{d\Omega}(Q) = \frac{\Delta\rho_z{}^2}{N_A}(S_D{}^I + S_H{}^I + S_{DD}{}^{II} + S_{HH}{}^{II} - 2S_{DH}{}^{II}) \tag{9}$$

Under the assumption that the correlations between D chains, between H chains, and between H and D chains are equal the distinct contribution cancels and, under the further assumption that the form factors of both chains are identical eq 9 simplifies to

$$\frac{d\Sigma}{d\Omega}(Q) = \frac{\Delta\rho_z{}^2}{N_A}2S_D{}^I \tag{10}$$

With $S_D{}^I$ written in the normalized form

$$S_D{}^I = \frac{\phi}{2}V_W P(Q) \tag{11}$$

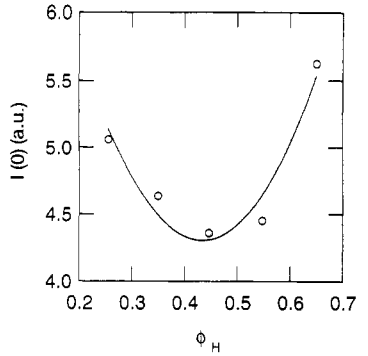

Figure 1. Scattered intensity at $Q = 0$ of the isotopic star mixture, PB6407, in protonated and deuterated methylcyclohexane as a function of the volume fraction of the protonated solvent. The solid line represents a parabola fit. The minimum indicates zero average contrast.

the coherent macroscopic scattering cross section is directly related to the form factor at each concentration:

$$\frac{d\Sigma}{d\Omega}(Q) = \frac{\Delta\rho_z^2}{N_A}\phi V_W P(Q) \tag{12}$$

The SANS measurements on samples PI8 and PI18 were performed at the D17 spectrometer at the Institute Laue Langevin in Grenoble, France. The experimental conditions have been published elsewhere.[12] All other SANS experiments were carried out at the NG7 30m machine at the National Institute of Standards and Technology in Gaithersburg, MD. In order to obtain the form factors in the limit of zero concentration, measurements at polymer volume fractions of $\phi = 0.01$, 0.005, and 0.0025 were typically performed. Methylcyclohexane-d_{14} was used as solvent.

In the case of the zero average contrast experiment 50 vol % blends of the protonated and the deuterated stars were prepared. In order to match the average scattering length density of the blends, five isotopic mixtures of methylcyclohexane ranging from 25% to 65% of the protonated species were examined in a preliminary test (see Figure 1). At constant polymer concentration (2%) a minimum in the forward scattering indicated zero average contrast at 43.2% (PB 64 arm star) and 45.6% (PI 18 arm star) methylcyclohexane-h_{14}, which are close to the calculated values of 45% (PB star) and 43% (PI star), respectively. Using these experimentally determined solvent compositions polymer solutions were prepared ranging in concentration from $0.01 \leq \phi \leq 0.30$.

Samples at low concentrations ($\phi \leq 0.01$) were measured in 5 mm quartz cells. Transmission coefficients are typically around 60%. For samples under zero average contrast conditions 2 mm cells were used. For those samples constant values for the transmissions of 0.49 (PI star) and 0.52 (PB star) were determined.

SANS experiments were performed at room temperature using different spectrometer setups. Depending on the sample a maximum range of the scattering wave vector of $0.005\ \text{Å}^{-1} \leq Q \leq 0.13\ \text{Å}^{-1}$ was covered. This was achieved by using either a fixed sample to detector distance with an offset of 30 cm or with a centered detector but two different distances. The wavelength was 5.5 or 7 Å with a spread of $\Delta\lambda/\lambda = 20\%$. During the measurements on PB6415 and PB128 and the experiments under zero average contrast the wavelength spread was 14%. The raw data were corrected for background, empty cell, and solvent. Absolute scattering cross sections were obtained by calibration with a silica gel secondary standard and for short distances additionally by a water standard:[30]

$$\frac{d\Sigma(Q)}{d\Omega} = \frac{I(Q)}{I_S(0)}\frac{\text{MON}_S}{\text{MON}}\frac{d_S}{d}\frac{T_S}{T}\left(\frac{d\Sigma(0)}{d\Omega}\right)_S \tag{13}$$

where S refers to the standard. MON denotes the total monitor count, d the cell thickness, and T the transmission. $I(Q)$ is the scattered intensity, and $I_S(0)$ is the measured intensity of the standard at $Q = 0$. $d\Sigma(0)/d\Omega = 32\ \text{cm}^{-1}$ for the silica gel standard. In the case of water $d\Sigma(0)/d\Omega = 0.777\ \text{cm}^{-1}$ at 5.5 Å and $0.828\ \text{cm}^{-1}$ at 7 Å. Finally, incoherent scattering contributions caused by the protonated polymer were calculated and subtracted.

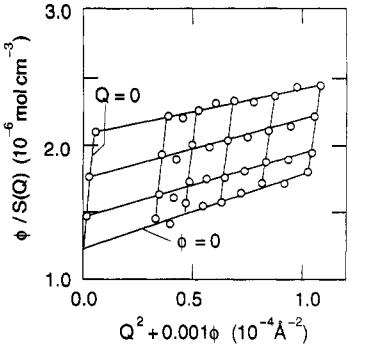

Figure 2. Concentration dependent Zimm plot of PB12807. Concentrations: $\phi = 0.25$, 0.5, and 1%.

3. Results

The scattering cross sections of the experiment under standard conditions, $d\Sigma(Q)/d\Omega$, were transformed to $S(Q)$ according to eq 1. The scattering function obtained revealed concentration dependent differences at low Q. In order to determine the star form factors, $P(Q)$, the scattering curves were extrapolated to infinite dilution using a concentration dependent Zimm plot. This was performed not only in the Guinier regime but also in the whole Q range, where the concentration dependent differences appeared. In the limit $\phi \to 0$ the scattering function is given by

$$\frac{1}{\phi}S(Q,\phi \to 0) = V_W P(Q) \tag{14}$$

In order to obtain proper form factors also at high Q the statistic was improved by averaging the data of all measured concentrations. This was possible since all scattering curves are identical in this Q range.

For a quantitative evaluation in the low Q regime the data were analyzed by the classical Zimm and Guinier method. No analysis was carried out on the stars PB3220 and PB3237 since the Guinier condition $QR_G < 1$ is not fulfilled in the Q range available. Representative for the stars, Figure 2 shows a Zimm plot of PB12807. According to the definition (eq 3), the plot yields the weight average molecular volume, V_W, from the intercept at $Q = 0$. By multiplication with the density of the polymer the molecular weights, M_W, were determined. They are included in Table 1. The good agreement with the light scattering data reveals the quality of the absolute calibration. The radii of gyration were obtained from the slope of the curve extrapolated to $\phi = 0$ with $P(Q) = 1 - Q^2R_G^2/3$. Radii of gyration were also obtained from Guinier plots, as shown in Figure 3 with $P(Q) = \exp(-Q^2R_G^2/3)$.

The results are listed in Tables 2 and 3. We found that the radii of gyration obtained by the two methods differ considerably from each other. This can be understood by the fact that close to the limit $QR_G = 1$ radii of gyration are overestimated by a Zimm and underestimated by a Guinier evaluation. Since the recording of data at sufficiently low Q was not possible, we have performed a correction of the Zimm plot according to a procedure given by Ullman.[31] This procedure is based on Gaussian coils but can also be used as a first order correction for other coil conformations. The corrected data are also listed in Tables 2 and 3. The new results lie now between the two extremes of Zimm and Guinier.

Star form factors are shown in a generalized Kratky representation in Figure 4. In this representation a peak occurs, which becomes more pronounced with the increas-

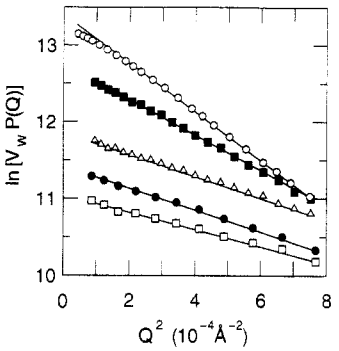

Figure 3. Guinier plots of form factors of stars PI8, PI18, PB3205, PB6407, and PB12807 (from bottom curve). Data of PI18 are offset by a factor of 0.97 for clarity. V_W is given in the units cm^3 mol^{-1}.

Table 2. Radii of Gyration, Step Height of Stars and Flory Exponent ν as a Function of the Number of Arms

	R_G/Å					
sample	Zimm	Guinier	Kratky	Zimm[a]	$P(0)/P(f^{1/2})$	ν^b
PB12807	111	86	109	105	877	0.67
PB6407	113	80	97	98	295	0.67
PB3205	88	64	72	79	119	0.68
PI18	82	67	75	74	36	0.65
PI8	69	58	67	65	6	0.64

[a] Zimm results corrected by the Ullman approximation. [b] Determined by a power law fit of the asymptotic range at high Q.

Table 3. Radii of Gyration of Star Polymers as a Function of the Number of Monomers per Arm

	R_G/Å					
sample	Zimm	Guinier	Kratky	Zimm[a]	LS[b]	$M_{N,arm}/M_{Mon}$
PB3205	88	64	72	79		100
PB3210	114	87	98	101	100	176
PB3220			153		145	359
PB3237			222		224	693
PB6407	113	80	97	98		119
PB6415	147	96	124	129		224
PI18	82	67	75	74		110

[a] Zimm results corrected by the Ullman approximation. [b] By light scattering in cyclohexane.[14]

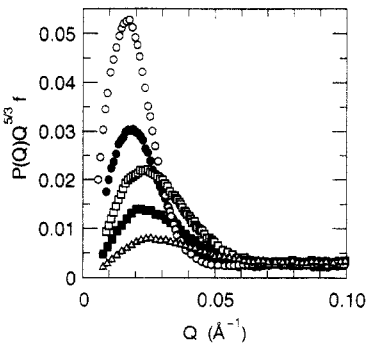

Figure 4. Form factors of stars PI8, PI18, PB3205, PB6407, and PB12807 (from bottom curve) in a generalized Kratky representation.

ing number of arms. The peak in a Kratky plot is a characteristic feature of star form factors and does not appear for linear polymers.[5,6,11,32] From the peak position, Q_{max}, radii of gyration can be determined by approximating the true form factor by the Gaussian star form factor[6,33] evaluated by Benoit:[17]

$$P(Q) = \frac{2}{fv^4}\left[v^2 - [1 - \exp(-v^2)] + \frac{f-1}{2}[1 - \exp(-v^2)]^2\right] \quad (15)$$

with

$$v = \sqrt{\frac{f}{3f-2}}QR_G \quad (16)$$

From the first derivative of $Q^2P(Q)$ the peak maximum was calculated to lie between $v = 1.1$ and $v = 1.3$, depending on f. R_G values obtained from this peak position are also listed in Tables 2 and 3. Although this method is strictly valid only for the Θ state the values obtained are close to those from the Zimm evaluation corrected according to Ullman. Thus, for those stars, where the Zimm regime could not be accessed, it appears to be justified to take R_G values from the Kratky evaluation. As seen in Table 3 the Kratky and corrected Zimm values of R_G are also in good agreement with light scattering results obtained in cyclohexane.[14]

In order to compare the scattering from star polymers of different functionalities and molecular weights, in Figure 5 we present data in a scaling representation. The abscissa was scaled with R_G; the scaling of the ordinate was done such that in the asymptotic high Q limit all data should collapse on one curve: At low Q the scattering of all arms superimposes coherently—the intensity becomes proportional to $(Nf)^2$, where N is the number of monomers per arm—while at high Q, according to eq 15, we have incoherent superposition of the arm scattering, rendering $I \sim N^2f/v^2$. Thus the normalized intensity should be scaled by f, or $V_WP(Q)/N \sim NfP(Q)/N$. The number of monomers per arm was calculated by $N = M_{N,arm}/M_{Mon}$ using for $M_{N,arm}$ either the results of the osmometry or the SEC analysis. M_{Mon} is the molecular weight of isoprene or butadiene, respectively. The PI stars were adapted to the PB stars by the ratio of the monomer volumes, $V_{PB}/V_{PI} = 0.8$. Further small deviations at high Q (maximum relative change 11%) were adjusted using shift factors. The magnitude of these corrections is within the uncertainty of absolute calibration (for values see Figure 5). Figure 5 demonstrates the strong enhancement of the low Q scattering if the functionality is increased. Figure 6A displays the form factors of a series of $f = 32$ arm stars spanning a M_W range of about a factor of 7. Scaling them with R_G and N leads to the mastercurve shown in Figure 6B—stars with different M_W and equal f are self-similar and even for the lowest M_W ($M_{N,arm} = 5400$) no anomalies due to the crowded center are visible.

Under zero average contrast conditions the form factors are directly related to the scattering cross section since interparticle contributions cancel (eq 12). The scattering curves obtained reveal that at low concentrations the form factors of the 64 and 18 arm stars are nearly independent of ϕ, while at higher concentrations deviations occur. Figure 7A displays form factors for some representative concentrations of the PI18 star. It can be seen that all curves start from the same intensity level at low Q. With increasing scattering vector the intensity rises with growing concentration, leading to a shift in $P(Q)$ at intermediate Q, before the curves start to merge again in the asymptotic range. Since the intensity enhancement commences in the Guinier regime, the changes in $P(Q)$ can be attributed to a decrease of the radius of gyration of the star. We have determined R_G by scaling Q such that the form factors at each concentration superpose onto the curve of the lowest concentration, as presented in Figure 7B. The results for R_G are shown in Table 4.

As demonstrated by Figure 8, the concentration dependence of the 64 arm star form factor behaves qualitatively different. Here the initial part of $P(Q)$ is plotted in a Guinier representation. Independent of ϕ, $P(Q)$ displays a uniform slope at $QR_G < 1$. The curves start to diverge only at higher Q. Apparently, the changes in $P(Q)$

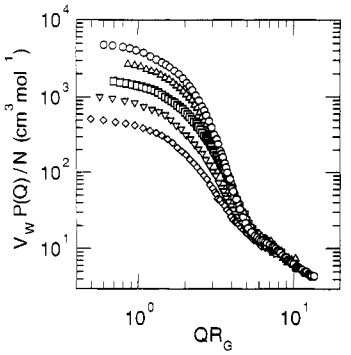

Figure 5. Form factors of stars PI8, PI18, PB3205, PB6407, and PB12807 (from bottom curve) in a double logarithmic representation. Data are scaled by the polymer volume, V_W, and by the number of monomers per arm, N. Additional shift factors: (PI8) 1.08; (PI18) 1.05; (PB32) 1.11; (PB64) 0.98; (PB128) 0.98. The abscissa was scaled by the radius of gyration, R_G, of the stars (Zimm results corrected according to Ullman).

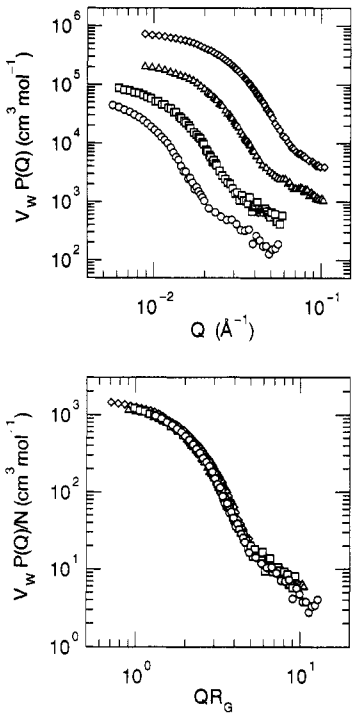

Figure 6. (A, top) Form factors of 32 arm stars with different molecular weights. From bottom: PB3237, PB3220, PB3210, and PB3205. (B, bottom) Self-similarity of the 32 arm stars demonstrated by scaling with the radius of gyration, R_G, and the number of monomers per arm, N.

are *not* due to a total shrinkage of the molecule but must originate from structural changes at a smaller scale without affecting the overall dimensions. Consequently, the evaluation of the radii of gyration by the Zimm method yields constant values over the whole concentration range (see Table 4). We note that a comparison between the form factor of the 1% solution of the zero average contrast experiment and the $\phi = 0$ extrapolated form factor of the experiment under standard conditions reveals a good agreement of the shape of $P(Q)$. However, deviations in the intensity were obtained, which might be due to errors in absolute normalization in the zero average contrast experiment. For the 18 arm star the form factor of the zero average contrast experiment differs by a factor of 1.31 from the form factor at $\phi = 0$, while in the case of the 64 arm star the intensity is lower by a factor of 0.79. These deviations can be caused by small differences in molecular volume between the two isotopic polymer species and by small errors in contrast.

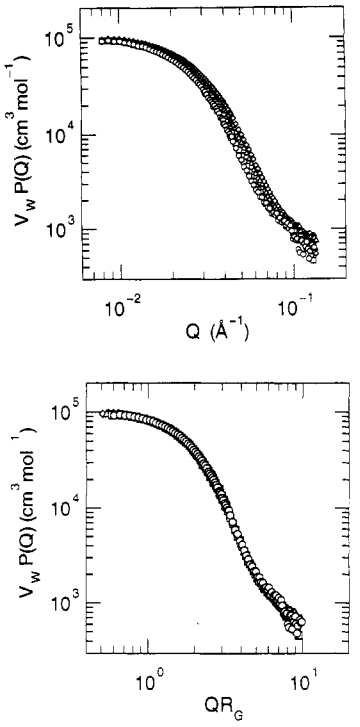

Figure 7. (A, top) SANS results of the zero average contrast experiment for the star mixture PI18/PI18D at various concentrations: $\phi = 5\%, 10\%, 15\%$, and 30% (from bottom curve). (B, bottom) Rescaling of the concentration dependent SANS form factors to a common mastercurve determining thereby the radius of gyration for each concentration.

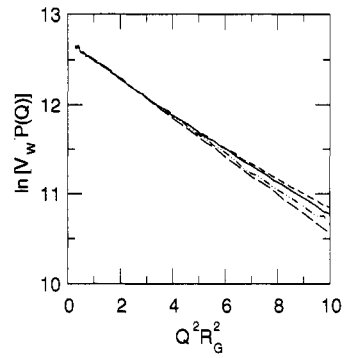

Figure 8. Guinier plot of the initial part of the 64-arm star form factors from the zero average contrast experiment for some representative concentrations: (lower dashed line) $\phi = 1.06\%$; (point dashed line) $\phi = 10\%$; (solid line) $\phi = 19.7\%$; (upper dashed line) $\phi = 29.8\%$. V_W in cm^3 mol^{-1}.

Table 4. Radii of Gyration as a Function of Concentration

PI18/PI18D		PB6407/PB6407D	
ϕ	R_G[a]/Å	ϕ	R_G[b]/Å
1.10	76.7	1.06	98.4
2.45	76.1	2.61	98.4
5.00	75.5	5.23	101.3
7.61	74.4	7.70	102.9
10.00	73.1	10.25	101.8
14.85	70.1	13.40	102.4
19.70	67.5	18.50	102.1
24.90	65.2	22.00	101.6
30.17	63.9	29.80	105.5

[a] Radii of gyration were obtained from scaling the form factors at different concntrations onto a master curve. [b] By Zimm analysis.

4. Discussion

4.1. Scaling Analysis. The radii of gyration evaluated from the form factors of the stars provide the opportunity to test scaling laws given by the Daoud–Cotton model.[20] The model divides the star into three different regions: the swollen region, the unswollen region, and the core. For

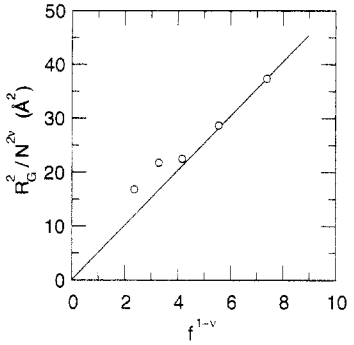

Figure 9. Plot of $R_G/N^{2\nu}$ for the largest stars of each functionality as a funciton of $f^{1-\nu}$ (ν = 0.588).

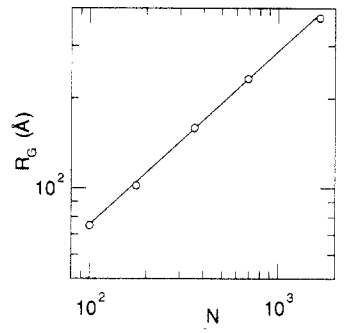

Figure 10. Double logarithmic plot of R_G vs N for 32 arm stars. The radius of gyration of the highest molecular weight star (N = 1659; R_G = 375 Å) in this plot was taken from ref 14. The solid line displays the expected scaling behavior in good solvents (ν = 0.588).

the case of long arms the swollen regime dominates, resulting in the following R_G dependence on f and N:

$$R_G^2 \sim N^{2\nu} f^{1-\nu} \tag{17}$$

where ν denotes the Flory exponent. First we analyze the radii of gyration with respect to the predicted functionality dependence. For this purpose we used the R_G values from the largest stars investigated, taking the Ullman corrected data where available. We note that results are rather sensitive to small uncertainties in R_G. Figure 9 shows a plot of R_G^2 divided by $N^{2\nu}$ as a function of $f^{1-\nu}$. Since the characteristic ratios of PI and PB are similar, the data can be compared directly, if we assume that the excluded volume parameters are the same for PI and PB in methylcyclohexane which is regarded as an athermal solvent for both types of polymers. In the diagram the solid line represents the expected scaling behavior for $1 - \nu = 0.41$. It can be seen that in the case of the high functionality stars the predicted scaling is rather well verified, while larger deviations are found for the 8 and 18 arm stars. Partly, this disagreement may arise from the comparison of two different types of polymers. On the other hand deviations for stars with low functionalities were already observed by MD simulation.[23] It was related to crossover effects between the scaling of linear polymers (f = 1, 2) and star polymers ($f \gg 1$). Our result fits well to the findings of Roovers et al.[15] for higher molecular weight stars. They determined radii of gyration by light scattering in cyclohexane.

In order to determine the N dependence of the radius of gyration at constant f, we plot R_G versus N for the 32 arm star series shown in Figure 10. Radii of gyration for the stars PB3220 and PB3237 were taken from the analysis of the Kratky maximum, which was shown to be an accurate method for the determination of R_G of the stars. The plot agrees well with the expected scaling of swollen polymer which is displayed by a solid line of slope ν = 0.588.

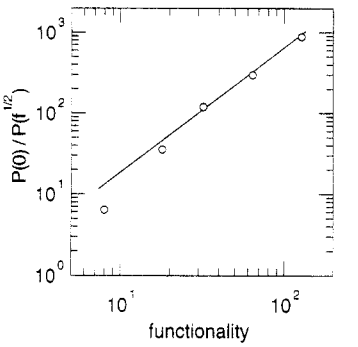

Figure 11. Double logarithmic representation of the step height, $P(0)/P(f^{1/2})$, as a function of f. The solid line displays the expected scaling behavior proportional to $f^{3/2}$.

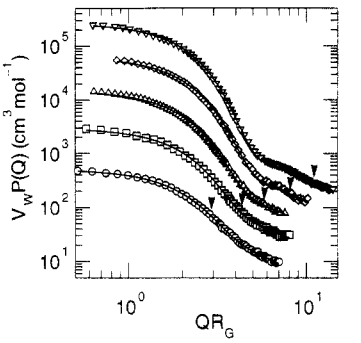

Figure 12. Form factors of stars PI8, PI18, P13205, PB6407, and PB12807 (from bottom curve) offset by a multiplicative constant. Arrows indicate the onset of the asymptotic regime according to $QR_G \sim f^{1/2}$. Solid lines represent fits with eq 22.

Another scaling property is the intensity drop between $P(Q = 0)$ and $P(Q = \xi(R_G)^{-1})$, as seen in Figure 5, where $\xi(R_G)$ is the outer blob size and $P(Q = \xi(R_G)^{-1})$ denotes the onset of the asymptotic regime. Following the considerations of Richter et al.,[7] one can express the intensity at $Q = \xi(R_G)^{-1}$ as $n_b[(\xi/\sigma)^{1/\nu}]^2$, representing the incoherent superposition of the coherent scattering from within the blobs. $n_b \sim (R_G/\xi)^3$ is the number of blobs and $(\xi/\sigma)^{1/\nu}$ the number of segments per blob with σ the segment length. At $Q = 0$ the scattering intensity of the whole star can be written as $[n_b(\xi/\sigma)^{1/\nu}]^2$, since all contributions add coherently. Taking into account that $\xi \sim R_G f^{-1/2}$, these considerations result in the following power law:

$$\frac{[(R_G/\xi)^3(\xi/\sigma)^{1/\nu}]^2}{(R_G/\xi)^3(\xi/\sigma)^{2/\nu}} \sim f^{3/2} \tag{18}$$

In order to test this scaling behavior the ratio $P(0)/P(QR_G = f^{1/2})$ was determined (values see Table 2) and plotted versus f, as displayed in Figure 11. The $f^{3/2}$ scaling of the step height is well confirmed for large f, while deviations are visible for low functionalities. It should be mentioned that $QR_G = f^{1/2}$ is not identical with the position of the break in the form factors at high Q. This is shown in Figure 12, where the positions of $f^{1/2}$ are indicated by arrows. In particular in the case of the f = 8 arm star it is obvious that $P(Q)$ has not yet developed the typical star profile, rendering the high f scaling law inapplicable.

4.2. Form Factors at Zero Concentration. In the present section the full Q dependence of the form factor will be considered. Schematically, three different scaling regimes come into question: The Guinier regime at $QR_G < 1$, the asymptotic regime at $Q\xi(R_G) > 1$, and the intermediate regime. For $Q < R_G^{-1}$ the total scattering of one star is given by $P(Q) = 1 - Q^2R_G^2/3$. For distances smaller than the blob size, $Q > \xi(R_G)^{-1}$, the scattering is determined by correlations of the excluded volume type

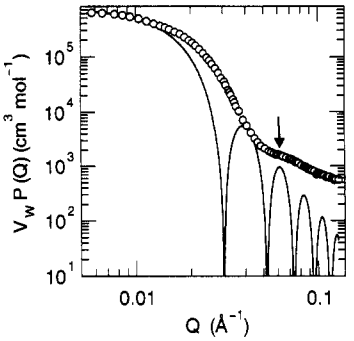

Figure 13. Form factors of the 128 arm star and a hard sphere calculated by eq 19. The radius of the sphere was taken as $(5/3)^{1/2}R_{G,star}$. The arrow marks the secondary maximum present in the star data.

which implies a $Q^{-1/\nu}$ dependence of $P(Q)$. Because of the limited number of data points in the appropriate Q range the results obtained for ν are relatively uncertain. However, power law fits at high Q clearly yield higher values for ν than theoretically expected (values see Table 2). This finding is in good agreement with former SANS experiments[6,7] and the MD simulation.[23] It was associated with a stretched configuration of the chains in star polymers.

In order to connect the scaling regimes at low and high Q the intensity has to drop in the intermediate Q range between $[(R_G/\xi)^3(\xi/\sigma)^{1/\nu}]^2$ and $(R_G/\xi)^3(\xi/\sigma)^{2/\nu}$. It can be seen from Figure 12 that the descent proceeds in a rather small Q range and becomes steeper with growing functionality. In the limit of a very high arm number the form factor of a star should approach that of a sphere.

Figure 13 shows the form factor of the 128 arm star together with $P(Q)$ of a sphere. The sphere form factor was calculated according to

$$P(Q) = \left(\frac{3}{\upsilon^3}(\sin\upsilon - \upsilon\cos\upsilon)\right)^2 \tag{19}$$

where $\upsilon = QR$, R was taken as $(5/3)^{1/2}R_{G,star}$. A typical feature of the hard sphere form factor is the Q^{-4}–Porod envelope for sharp interfaces. A comparison between star and sphere form factors shows that $P(Q)$ of the star envelopes the sphere form factor, covering about two of its oscillations before the scattering is dominated by the scattering from inside the blobs. Obviously, an intermediate power law decay is not exhibited, and consequently, one cannot draw conclusions about a star surface. On the other hand the form factors of the 64 and 128 arm stars exhibit a shallow peak in the asymptotic range. The position of this peak coincides with the position of the third oscillation of the sphere form factor, as marked by an arrow in Figure 13. Thus the stars assume more and more a spherical shape with a relatively sharp density cutoff at the periphery of the star.

Now we compare our results with the form factors from the MD simulation of Grest et al.[23] They present their results in terms of $Q\sigma$, where σ is the segment length. Therefore, in order to compare, we have scaled our data accordingly, estimating the segment length from $\sigma = 6^{1/2}R_G/(nN)^\nu$ (n = 3.86: number of main chain bonds per monomer). The intensity was adjusted using a constant shift factor for all scattering curves such that a comparison between simulated and measured stars of a similar number of arms becomes possible. The resulting plot is shown in Figure 14. In general we obtain good agreement, though in detail some deviations appear. The simulated form factor at f = 10 stretches out to larger Q values before it breaks to the asymptotic regime. This behavior tends to change with increasing f where the simulated data decay slightly more rapidly than the experimental results.

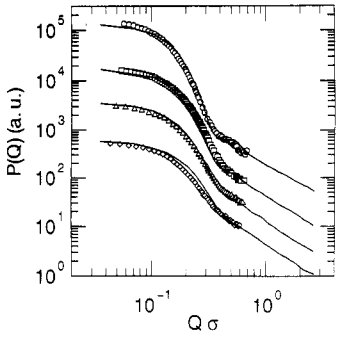

Figure 14. Form factors of stars PI8, PI18, PB3205, and PB6407 (from bottom curve) scaled by a factor such that they match simulated stars (solid lines) with 10, 20, 30, and 50 arms each containing 50 segments. Q was scaled by the segment length, σ, as pointed out in the text.

Furthermore, the secondary maximum seems to be more pronounced in the simulation than in the experiment. Seemingly, for large f the simulated stars assume a more developed sphere conformation. This may be due to the fact that the simulated stars consist of rather short arms (N = 50). For this case a considerable stretching of the arms is present (ν = 0.65), which implies a sharper density cutoff at the periphery of the star. Apparently, the scattering profile of larger stars is smeared by a more fuzzy edge.

In order to arrive at an approximation for the form factor of a star polymer, we consider that a star is governed by two different length scales: the overall size R_G and the correlation length or blob size ξ, where the granular polymer structure becomes important. At length scales $r \sim R_G$ the star is described by its average monomer density distribution $\rho(r)$, while at scales $r < \xi$ the correlations within a single chain in a good solvent dominate. Thus, the overall pair correlation function may be written as

$$G(r) = \begin{cases} \sim \int \rho(r')\rho(r-r')\,\mathrm{d}^3r' & r \approx R_G \\ \sim \sigma^{-1/\nu}r^{1/\nu-3} & r \le \xi \end{cases} \tag{20}$$

Recently, Dozier et al.[9] presented an approximation to eq 20. In order to assure the correct behavior in the Guinier regime, they described the long range correlations by a Gaussian, giving rise to the proper radius of gyration. The polymer type short range correlations were taken into account by the correlation function of a swollen chain (eq 20), including a cutoff function $\exp(-r/\xi)$, where ξ is an average blob size. Since both contributions exhibit their decay on well separated length scales, the total correlation function was written as a sum of both

$$G(r) = c_1\left(\frac{\pi}{R_G}\right)^3 \exp\left(-\frac{3r^2}{4R_G^2}\right) + c_2\exp(-r/\xi)\left(\frac{r}{\sigma}\right)^{1/\nu} r^{-3} \tag{21}$$

Thereby, c_1 and c_2 are numerical constants. Fourier transformation leads to the scattering function

$$V_W P(Q) = V_W \exp\left(-\frac{Q^2R_G^2}{3}\right) + \frac{\alpha}{Q\xi}\frac{\sin[\mu\tan^{-1}(Q\xi)]}{(1+(Q\xi)^2)^{\mu/2}} \tag{22}$$

where $V_W = \upsilon_p Nf$, $\mu = 1/\nu - 1$, and $\alpha \sim \upsilon_p(\xi/\sigma)^{1/\nu} \sim \upsilon_p Nf^{-1/2}$. Note that according to eq 22 again the ratio of the forward and the blob scattering obeys the $f^{3/2}$ law (eq 18). Equation 22 was fitted to the measured form factors by varying V_W, α, R_G, and ξ. ν was set to $^3/_5$. Using this ν, we obtained the best fits. This might be an indication that the power law with ν = 0.67 may be partly due to coherency effects arising from the superposition of scattering of different

Table 5. Fit Parameters[a] Obtained by Equation 22

sample	$10^{-3}V_W$/cm^3 mol^{-1}	R_G/Å	ζ/Å	α/cm^3 mol^{-1}
PI8	56	62	44	1217
PI18	128	68	30	695
PB3205	145	66	28	377
PB3210	235	91	35	703
PB3220	505	140	61	1580
PB3237	923	199	102	2830
PB6407	366	85	31	444
PB6415	722	113	45	849
PB12807	655	97	27	335

[a] ν was taken as $^3/_5$.

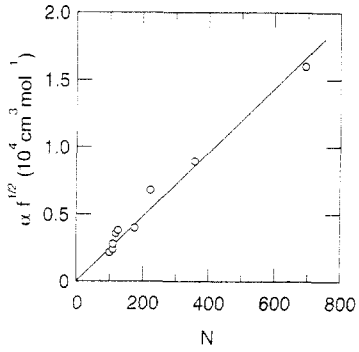

Figure 15. Plot of the intensity parameter $\alpha f^{1/2}$ (eq 22, Table 5) vs N. The solid line displays the expected linear behavior.

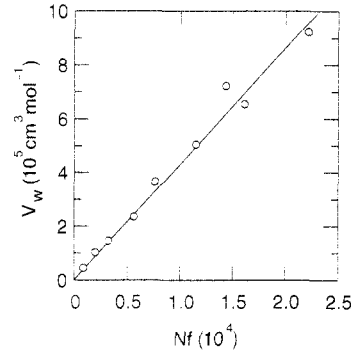

Figure 16. Plot of the fit parameter (eq 22) V_W as a function of Nf. The solid line presents the required linear relationship.

blobs. In order not to be influenced by the secondary maximum in the experimental form factor which is not contained in eq 22, data points in the neighborhood of this feature were not considered. The fits are displayed as solid lines in Figure 12. Results for V_W, R_G, ξ, and α are listed in Table 5. Figure 15 investigates the dependence of α on N. For this purpose $\alpha f^{1/2}$ is displayed against N. The intensity parameter α was corrected with regard to the differences in monomer volume between PI and PB. The plot reveals that the scaling requirement is rather well verified. Figure 16 presents a consistency check with respect to V_W, the star volume. As required, the fitted V_W increases linearly with Nf. Finally, Figure 17 displays the correlation between R_G and ξ. The plot of R_G/ξ as a function of $f^{1/2}$ reveals only fair agreement with the scaling prediction. Though good descriptions of the scattering curves are obtained, eq 22 is based on an average blob size and does not consider a blob size increasing with the distance from the star center.

Figure 18 shows a generalized Kratky representation of the 18 arm star form factor. The data are fitted by the Benoit function (eq 15). The peak is well described by the fit, but as expected, significant deviations occur at higher Q. Here the theoretical curve decreases continuously and does not flow into the characteristic $Q^{-5/3}$ plateau since it does not take into account self-avoiding walk statistics. The dashed line in Figure 18 represents a fit of an

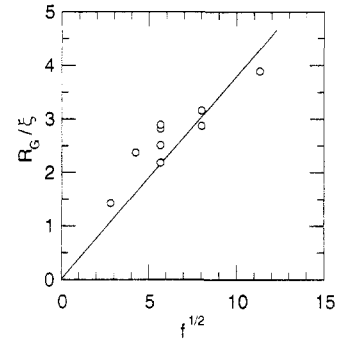

Figure 17. Radii of gyration (Tables 2 and 3) divided by the fitted correlation length ξ as a function of $f^{1/2}$. The solid line presents the Daoud–Cotton prediction.

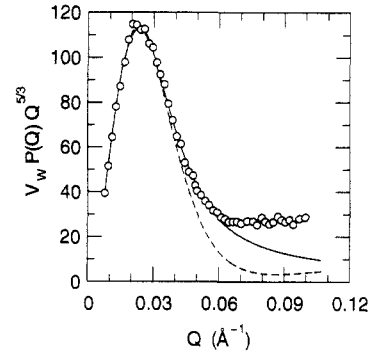

Figure 18. Generalized Kratky representation of the 18 arm star form factor. The solid line represents a fit with eq 15 (Gaussian star model); the dashed line, a fit of the swollen star model of Alessandrini and Carignano. For the fitting procedure the data in the asymptotic regime were taken out.

expression given by Alessandrini and Carignano:[18]

$$P(y) = f(y)[1 + A_1(e^{-A_2y} - 1) + A_3y + A_4y^2] \quad (23)$$

This formula represents a best nonlinear fit of an equation derived by renormalization group techniques, which was developed for stars in order to incorporate the excluded volume effects of monomers in a good solvent. In eq 23 $y = 3/4(f/(3f-2))Q^2R_G^2$ and $f(y)$ is the Benoit function (eq 15) with variable y. $A_1, ..., A_4$ are f dependent parameters. For $f = 18$, $A_1 = 1.1$, $A_2 = 0.41$, $A_3 = 0.015$, and $A_4 = -2 \times 10^{-5}$. A comparison with the experimental data reveals an increasing deviation at $Q > Q_{max}$. The intensity of the theoretical curve decreases more rapidly and, thereby, overestimates the step between the peak maximum and the high Q plateau. Here the $Q^{-5/3}$ behavior is well represented. However, the results show that both theories are limited in describing the experimental star form factors.

4.3. Concentration Dependence of the Form Factors. According to Daoud and Cotton[20] a semidilute solution of star polymers resembles that of linear polymers containing small islands of star centers. For concentrations much higher than the overlap concentration ϕ^*, the star centers are small and the ϕ dependence for linear polymers[34] is expected also to hold for stars:

$$R_G \sim \sigma N^{1/2}(\phi/\phi^*)^{-(2\nu-1)/2(3\nu-1)} \quad (24)$$

yielding $R_G \sim \sigma N^{1/2}(\phi/\phi^*)^{-1/8}$ for $\nu = {}^3/_5$. For concentrations close to the overlap concentration star centers are extended and the behavior is dominated by single stars. In this case the model yields a $\phi^{-3/4}$ dependence of the radius of gyration. In order to demonstrate the influence of the concentration on the star size we have plotted R_G of the 18 arm star as a function of ϕ in Figure 19. While the star size is constant up to a concentration of $\phi = 10\%$,

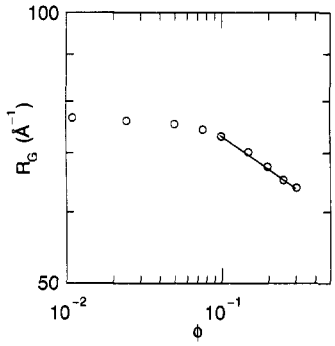

Figure 19. Double logarithmic plot of the radius of gyration versus concentration of the 18 arm star. The solid line displays the concentration behavior of linear polymer chains in a semidilute solution. The overlap concentration of this star was determined to be 10%.[12]

which is known to be the overlap concentration,[12] a shrinkage of the star is observed at higher ϕ. In accord with the scaling behavior for linear polymers we have obtained a slope of −0.125 in the semidilute range. However, the plot does not reveal any sign of the $\phi^{-3/4}$ dependence.

5. Conclusion

In this paper we have presented a comprehensive study on single star form factors as a function of molecular weight, functionality, and concentration by SANS in a good solvent. Since interparticle effects cannot be ignored, the form factors were determined by extrapolating scattered intensities to zero concentration. The configurational properties of the stars were found to be in good agreement with the Daoud–Cotton scaling predictions. Furthermore, we have shown that the zero average contrast experiment is a convenient technique to measure the concentration dependence of $P(Q)$. Thereby, a shrinkage of an 18 arm star was observed in semidilute solution to follow a scaling law consistent with that of linear polymers.

A prevailing signature of the star form factors is the intensity drop from the low Q plateau to the high Q power law regime which increases with increasing functionality. On the basis of considerations on the coherent and incoherent superposition of blob scattering, the intensity drop should follow an $f^{3/2}$ law which could be verified by the experiments. On a series of 32 arm stars we demonstrated that the arm length does not influence the shape of $P(Q)$. Another important observation concerns the tendency toward more spherelike form factors if the functionality increases. Though not as pronounced as in computer simulations for the 64 and 128 arm stars, we found clear evidence for a secondary maximum in the form factor resembling the third oscillation of the corresponding sphere form factor.

Finally, we discussed the measured form factors in terms of an approximative analytic form factor for Daoud–Cotton stars. Not only do we obtain a quantitative description of the measured intensity patterns, but also the appropriate scaling relations are fulfilled by the model parameters.

Acknowledgment. We thank the National Institute of Standards and Technology and the Institut Laue-Langevin for providing the SANS beam time. We are grateful to Dr. M. Monkenbusch for clarifying discussions.

References and Notes

(1) Huber, K.; Burchard, W.; Fetters, L. J. *Macromolecules* **1984**, *17*, 541.
(2) Huber, K.; Bantle, S.; Burchard, W.; Fetters, L. J. *Macromolecules* **1986**, *19*, 1404.
(3) Huber, K.; Burchard, W.; Bantle, S.; Fetters, L. J. *Polymer* **1987**, *28*, 1990.
(4) Huber, K.; Burchard, W.; Bantle, S.; Fetters, L. J. *Polymer* **1987**, *28*, 1997.
(5) Richter, D.; Stühn, B.; Ewen, B.; Nerger, D. *Phys. Rev. Lett.* **1987**, *58*, 2462.
(6) Richter, D.; Farago, B.; Huang, J. S.; Fetters, L. J.; Ewen, B. *Macromolecules* **1989**, *22*, 468.
(7) Richter, D.; Farago, B.; Fetters, L. J.; Huang, J. S.; Ewen, B. *Macromolecules* **1990**, *23*, 1845.
(8) Lantman, C. W.; Macknight, W. R.; Rennie, A. R.; Tassin, J. F.; Monnerie, L. *Macromolecules* **1990**, *23*, 836.
(9) Dozier, D. W.; Huang, J. S.; Fetters, L. J. *Macromolecules* **1991**, *24*, 2810.
(10) Stivala, S. S.; Khorramian, B. A.; Patel, A. *Polymer* **1986**, *27*, 517.
(11) Khorramian, B. A.; Stivala, S. S.; *Polym. Commun.* **1986**, *27*, 184.
(12) Willner, L.; Jucknischke, O.; Richter, D.; Farago, B.; Fetters, L. J.; Huang, J. S. *Europhys. Lett.* **1992**, *19*, 297.
(13) Adam, M.; Fetters, L. J.; Graessley, W. W.; Witten, T. A. *Macromolecules* **1991**, *24*, 2434.
(14) Zhou, L. L.; Hadjichristidis, N.; Toporowski, P. M.; Roovers, J. *Rubber Chem. Technol.* **1992**, *65*, 303.
(15) Roovers, J.; Zhou, L. L.; Toporowski, P. M.; van der Zwan, M.; Iatrou, H.; Hadjichristidis, N. *Macromolecules* **1993**, *26*, 4324.
(16) Benoit, H.; Hadziioannu, G. *Macromolecules* **1988**, *21*, 1449.
(17) Benoit, H. *J. Polym. Sci.* **1953**, *11*, 507.
(18) Alessandrini, J. L.; Carignano, M. A. *Macromolecules* **1992**, *25*, 1157.
(19) Allegra, G.; Colombo, E.; Ganazzoli, F. *Macromolecules* **1993**, *26*, 330.
(20) Daoud, M.; Cotton, J. P. *J. Phys.* **1982**, *43*, 531.
(21) Birshtein, T. M.; Zhulina, E. B. *Polymer* **1984**, *25*, 1453.
(22) Birshtein, T. M.; Zhulina, E. B.; Borisov, O. V. *Polymer* **1986**, *27*, 1078.
(23) Grest, G. S.; Kremer, K.; Witten, T. A.; *Macromolecules* **1987**, *20*, 1376.
(24) Hadjichristidis, N.; Fetters, L. J. *Macromolecules* **1980**, *13*, 191.
(25) Hadjichristidis, N.; Guyot, A.; Fetters, L. J. *Macromolecules* **1978**, *11*, 668.
(26) Zhou, L. L.; Roovers, J. *Macromolecules* **1993**, *26*, 963.
(27) Csiba, T.; Jannink, G.; Durand, D.; Papoular, R.; Lapp, A.; Auvray, L.; Boue, F.; Cotton, J. P.; Borsali, R. *J. Phys. II* **1991**, *1*, 381.
(28) Duval, M.; Picot, C.; Benmouna, M.; Benoit, H. *J. Phys.* **1988**, *49*, 1963.
(29) Borsali, R.; Benoit, H.; Legrand, J.-F.; Duval, M.; Picot, C.; Benmouna, M.; Farago, B. *Macromolecules* **1989**, *22*, 4119.
(30) SANS Data Reduction and Imaging Software; National Institute of Standards and Technology: Gaithersburg, MD 20899, June 11, 1993.
(31) Ullman, R. *J. Polym. Sci., Polym. Phys. Ed.* **1985**, *23*, 1477.
(32) Burchard, W. *Macromolecules* **1977**, *10*, 919.
(33) Willner, L.; Jucknischke, O.; Richter, D.; Fetters, L. J.; Huang, J. S.; Farago, B. *Makromol. Chem., Macromol. Symp.* **1992**, *61*, 122.
(34) Daoud, M.; Cotton, J. P.; Farnoux, B.; Jannink, G.; Sarma, G.; Benoit, H.; Duplessix, R.; Picot, C.; de Gennes, P. G. *Macromolecules* **1975**, *8*, 804.